POLITECNICO DI TORINO
Repository ISTITUZIONALE

Impact of Spread Spectrum Modulated Switching Noise on Feedback Operational Amplifiers

Original
Impact of Spread Spectrum Modulated Switching Noise on Feedback Operational Amplifiers / Serra, J., Fiori, F.. - STAMPA. - (2026), pp. 1-6. (International Symposium on Electromagnetic Compatibility (EMC Europe 2026) Praga (Cze) 31August - 4 September 2026).

Availability:
This version is available at: 11583/3012566 since: 2026-07-01T07:59:25Z

Publisher:
IEEE

Published
DOI:

Terms of use:

This article is made available under terms and conditions as specified in the corresponding bibliographic description in the repository

Publisher copyright
IEEE postprint/Author's Accepted Manuscript

©2026 IEEE. Personal use of this material is permitted. Permission from IEEE must be obtained for all other uses, in any current or future media, including reprinting/republishing this material for advertising or promotional purposes, creating new collecting works, for resale or lists, or reuse of any copyrighted component of this work in other works.

(Article begins on next page)

14 September 2026

Impact of Spread Spectrum Modulated Switching Noise on Feedback Operational Amplifiers

Jacopo Serra, Franco Fiori
Electronics and Telecom. Dpt.
Politecnico di Torino
Torino, Italy
Email: jacopo.serra@polito.it

***Abstract*—This paper investigates the susceptibility of operational amplifiers (OpAmps) to spread-spectrum–modulated switching noise in power ASICs. The fast commutation of large switching devices injects electric charges into the silicon substrate they share with other building blocks like the analog ones, that results in switching noise superimposed onto the nominal signals. While primarily present at high frequencies, the switching noise is also demodulated by the nonlinear devices in the analog section, generating in-band components.**
Since such disturbances are inherently synchronous with the PWM clock, any spread-spectrum modulation applied to the switching frequency directly shapes the substrate-coupled interference. Therefore, input-referred switching-interference waveforms are first derived using a simplified substrate-coupling model that captures the interaction between the power and analog/control sections. The disturbances are then shaped through spread-spectrum modulation, whose parameters are optimized for EMI reduction, and injected into a commercial operational amplifier using the Direct Power Injection (DPI) approach. Experimental results show that the spread-spectrum–modulated substrate noise is demodulated by the device under test, generating an in-band component at the modulation frequency.

***Index Terms*—Electromagnetic interference, Substrate Coupling, Spread Spectrum Modulation, Switching Noise Demodulation, DC/DC converters, ASICs, PMIC**

I. Introduction

The continuous scaling of electronic technologies has led to extremely integrated systems-on-chip combining multiple functionalities in a single die. The integration of analog, digital and power circuits on the same silicon die, driven by the demand for smaller, cheaper, and higher-performance devices, has however introduced serious intra-compatibility issues [1].
Substrate coupling is one of the primary sources of these compatibility issues. Switching activity in digital cores and power transistors injects noise into the substrate, which spreads through the chip affecting the performance of the other blocks, especially the analog ones [2], [3], [4]. Over the years, substantial effort has been devoted to understanding and mitigating substrate coupling. Most solutions focus either on technological isolation, such as guard rings and SOI processes, or on circuit-level strategies, including clock skewing and substrate transfer-function shaping [5]. While these approaches can significantly improve immunity in conventional designs, they are primarily tailored to low-power mixed-signal environments.
However, this scenario changes significantly in power ASICs, where the commutation of large power devices generates high-amplitude, repetitive disturbances often exceeding the noise levels observed in conventional digital or mixed-signal circuits [6]. Because these disturbances are inherently synchronized with the pulse-width modulator (PWM) switching period, any PWM modulation directly translates into a modulation of the coupled substrate noise. Spread-spectrum modulation (SSM), widely employed in DC/DC converters for electromagnetic interference (EMI) reduction [7], intentionally modulates the PWM frequency. Consequently, the substrate-coupled disturbance is itself modulated, raising the question of how such modulation impacts the susceptibility of analog building blocks.
The analysis follows a conventional design perspective, in which spread-spectrum parameters are optimized exclusively for EMI mitigation, neglecting potential intra-system effects. The coupling between the power stage and the analog section through the shared substrate is first characterized, and the resulting disturbances are subsequently used to assess the susceptibility of representative analog circuits.
The remainder of the paper is organized as follows. Section II analyzes substrate coupling in power ICs and derives representative switching-noise waveforms. Section III investigates three spread-spectrum modulations, namely sinusoidal, triangular, and PAM, and optimizes their parameters for EMI reduction. The demodulation mechanism in operational amplifiers is discussed in Section IV, followed by DPI measurements on a commercial OpAmp using the synthesized spread-spectrum–modulated switching noise in Section V. Finally, concluding remarks are provided in Section VI.

II. The substrate coupling problem in Power ASICs

This section investigates the intra-system compatibility of a power ASIC, for instance a DC/DC converter, where a switching leg in the power section acts as the aggressor and an OpAmp in the analog section as the victim. Ideally, the aggressor and the victim should be isolated, but in practice they are coupled through the shared substrate.
Over the last decades, substrate coupling has been widely

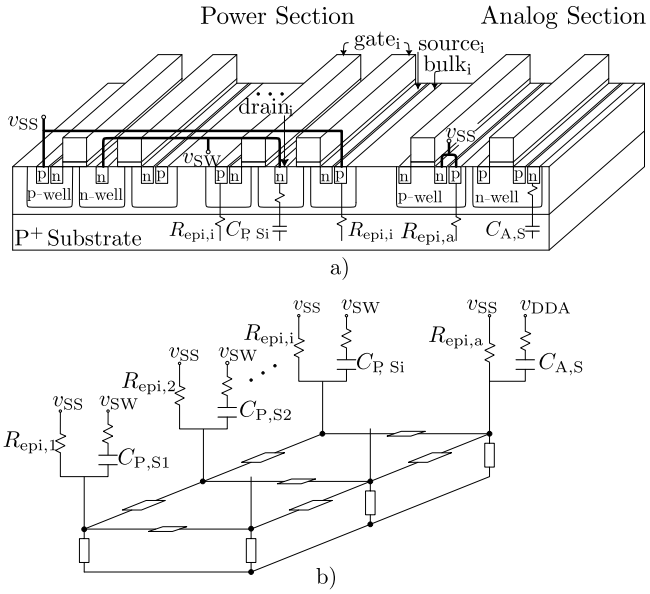

Fig. 1: Low-side LDMOS (aggressor) and analog circuits (victims) in an isolated CMOS process. (a) Cross section. (b) Macro model of the substrate coupling network.

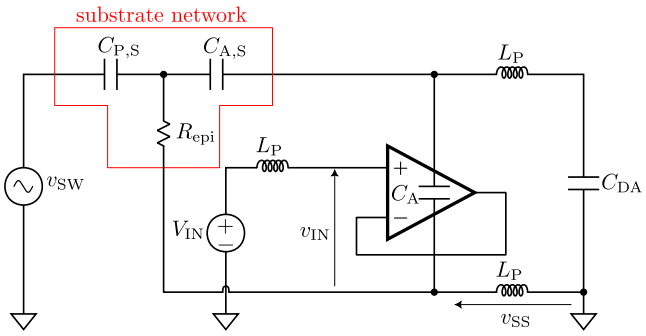

Fig. 2: Equivalent circuit used to study the propagation of the switching noise through the substrate.

TABLE I: CIRCUIT PARAMETERS

Parameter	Value	Parameter	Value
L_P	2.5 nH	$C_{A,S}$	2 pF
C_A	5 pF	R_{epi}	10 Ω
C_{DA}	100 nF	$C_{P,S}$	120 pF

investigated using numerical finite-difference or quasi-analytical methods. Although highly accurate and technology-independent, these approaches are computationally demanding in both extraction and simulation. For ICs fabricated on an epitaxial (EPI) substrate, however, compact macro-models provide an accurate and much simpler alternative, as shown in [8].

In this work, the macro-model approach is used to describe the aggressor switching leg, which consists of two lateral diffused (LD) NMOS transistors fabricated in a HV 350 nm CMOS process. Figure 1(a) shows the cross-section of the process. It comprises the switching leg low-side transistor, implemented as an array of unit devices, together with representative NMOS and PMOS victims. The associated substrate macro-model used to analyze the propagation of switching noise within the substrate is shown in Fig. 1(b). Specifically, each unit device is described by an equivalent RC network, where $C_{P,Si}$ is the capacitance due to the reverse-biased junction in the i-th drain and the resistances accounts for the epitaxial path to the substrate. The same equivalent network is used for the analog victim ($C_{A,S}$, and $R_{epi,a}$). To identify the worst-case scenario, the series resistance of $C_{P,Si}$ and $C_{A,S}$ is neglected. Moreover, the low-resistivity epi-substrate is treated as an equipotential node, making unit-device parasitics appear effectively in parallel ($C_{P,S}$ and R_{epi}). Using the previously introduced substrate macro-model, the equivalent circuit shown in Fig. 2 represents the coupling between the aggressor, the victim, and the substrate. It comprises the substrate network made of a star connection including the $C_{P,S}$, C_{AS}, and R_{epi}. Parasitic inductances introduced by package interconnects and bonding wires are included by L_P. Both on-chip and off-chip decoupling capacitors (C_A and C_{DA}, respectively) are included in the analog section, while their parasitic elements are omitted from the figure for clarity.

The switching-node voltage (v_{SW}) couples through the substrate to the analog ground (v_{SS}), where it appears as a noise component superimposed onto the nominal OpAmp input. This noise is evaluated in the time domain using the circuit of Fig. 2 with parameters from Tab. I. The switching-node voltage is modeled as a trapezoidal waveform with equal rise and fall times of $t_r = 1.5$ ns, amplitude $A = 5$ V, and duty cycle $\delta = 0.5$. The waveform approximates the switching-node voltage in a synchronous DC/DC buck converter. The time-domain results are shown in Fig. 3 for a switching frequency of f_{SW} = 10 MHz. Each commutation produces a bipolar spike lasting a few nanoseconds and reaching an amplitude of several hundred millivolts. The interference power delivered to a reference resistance R = 50 Ω is

$$P_{in} = \frac{1}{T}\int_0^T \frac{v_{SS}(t)^2}{R}dt, \qquad (1)$$

where $T = 1/f_{SW}$ is the switching period. For the waveform shown in Fig. 3, the resulting nominal interference power is P_{in} = -7 dBm.

III. Spread-Spectrum Modulation

In DC/DC converters, spread-spectrum modulation is employed to mitigate EMI by introducing a controller jitter in the instantaneous switching frequency [9].

Considering frequency modulation (FM) applied to a sinusoidal carrier, the modulated signal can be expressed as

$$s(t) = A \cdot cos\left(2\pi f_c t + 2\pi\Delta f \cdot \int_{-\infty}^{t} \xi(\tau)d\tau\right), \qquad (2)$$

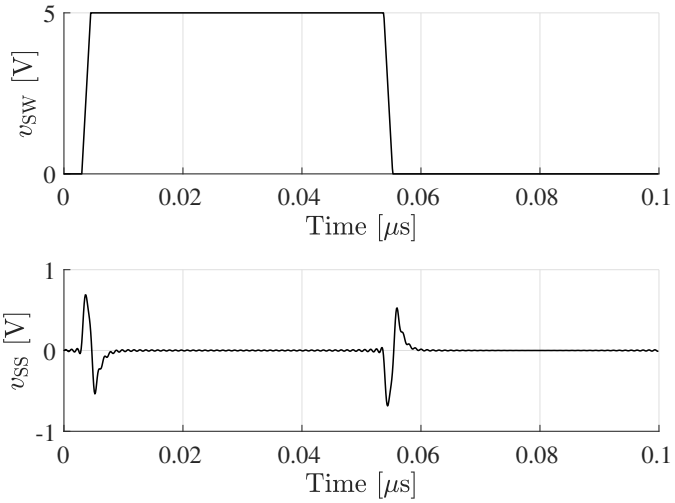

Fig. 3: Time domain analysis results. Switching-node voltage (v_{SW}) and induced analog ground disturbance (v_{SS}).

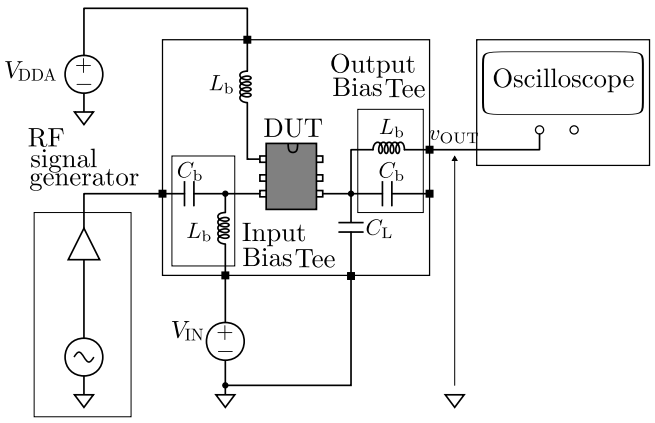

Fig. 4: Schematic view of the DPI setup considered to evaluate the susceptibility to EMI.

where f_{c} is the carrier frequency, Δf the frequency deviation, and $\xi(\tau)$ the normalized driving signal. Under FM, the instantaneous frequency of the carrier and its power spectrum are spread within Carson's bandwidth $[f_{\mathrm{c}} - \Delta f,\ f_{\mathrm{c}} + \Delta f]$. In this work, three driving signals are considered: sinusoidal, triangular and pulse-amplitude modulation (PAM) which is defined as

$$\xi(t) = \sum_{k} x_{\mathrm{k}} \cdot g(t - kT_{\mathrm{s}}), \tag{3}$$

where $x_{\mathrm{k}} \in [-1, 1]$ is a random-like sequence and $g(\tau)$ is a rectangular pulse of unit amplitude and duration T_{s}. A chaotic-map-based sequencer is adopted to generate unpredictable, non-periodic trajectories $\{x_{\mathrm{k}}\}$.

The EMI reduction performance depends on the spreading parameters, which are summarized by the modulation index

$$m = \Delta f / f_{\mathrm{m}}, \tag{4}$$

where $f_{\mathrm{m}} = 1/T_{\mathrm{m}}$ is the modulation frequency. In this investigation, for simplicity, the frequency deviation is set to $\Delta f = 0.1 f_{\mathrm{c}}$. The modulation parameters, for sinusoidal and triangular modulations, were optimized in terms of relative attenuation (RA) with respect to the unmodulated case, considering the EMI receiver emulator in [10] (RBW = 9 kHz) as a representative victim circuit. The analysis shows that, for each carrier frequency f_{c}, an optimal modulation index exists and is achieved when the modulation frequency satisfies $f_{\mathrm{m}} \approx \mathrm{RBW}$. For PAM, a T_{s} = 1/35 kHz was selected, leading to attenuation trends comparable to those observed with sinusoidal and triangular modulation.

IV. Switching Noise Demodulation in Analog Blocks

The switching noise generated by the DC/DC converter propagates to the analog blocks, where it appears as a high-frequency noise (HFN). Although the spectral components of such noise lie well above the bandwidth of the analog circuits and should therefore be rejected, in practice the HFN is demodulated, resulting in in-band disturbances that can significantly degrade circuit performance. This behavior mainly arises from the nonlinear characteristics of the active devices from which analog circuits are made of, and from the parasitic capacitances, which provide the memory required for its demodulation into in-band components [11]. The demodulated HFN propagates through the analog circuits, affecting the circuit's operating point and ultimately corrupting their output signal. Over the years, the demodulation of radio-frequency (RF) continuous-wave (CW) interference has been investigated in different analog circuits, including voltage references [12], linear voltage regulators [13], and operational amplifiers, as well as in digital circuits such as comparators [14].

Among analog circuits, operational amplifiers (OpAmps) are particularly susceptible to such RFI. In an operational amplifier, out-of-band RFI superimposed onto the nominal input signals is demodulated by the amplifier nonlinear input-stage. This mechanism has been extensively investigated by injecting a continuous-wave (CW) sinusoidal interference at the input, which has been shown to produce a DC shift at the output [15], [16]. While the CW-based approach provides valuable insight into the demodulation mechanism, it does not fully represent the characteristics of realistic interference, which is subject to rectification. Therefore, the susceptibility of the OpAmp is investigated using realistic substrate-coupled switching waveforms, modulated through spread-spectrum techniques and injected via the DPI setup.

V. Experimental results

The susceptibility of operational amplifiers to spread-spectrum–modulated switching interference is experimentally assessed by injecting the disturbance at the input pin through the DPI setup shown in Fig. 4 [17]. In this investigation, the Device Under Test (DUT) is a commercial OpAmp configured as a voltage follower, whose main parameters are listed in

TABLE II: OpAmp Parameters

Parameter	Value
A_d	100 dB
SR	0.6 V / µs
GBW	1.1 MHz
CMRR	85 dB
V_{off}	1 mV

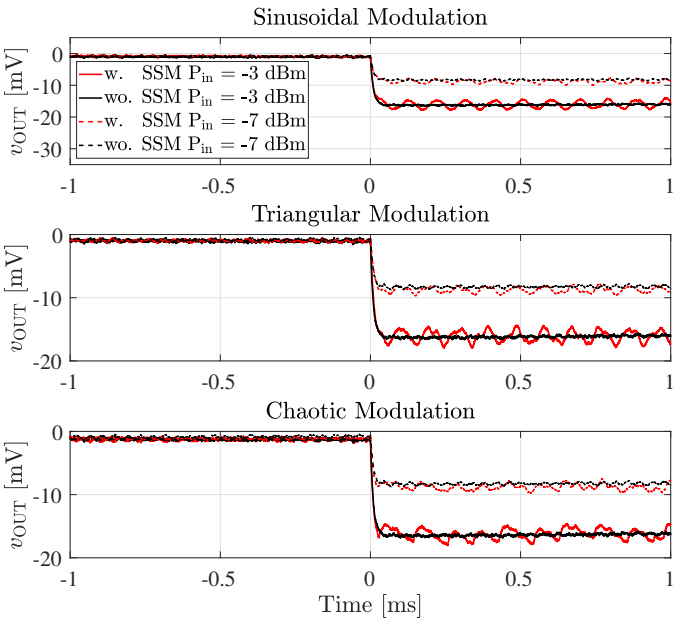

Fig. 5: Output voltages obtained injecting the switching noise interference at the OpAmp input pin, black lines identify the unmodulated interference while the red lines the modulated one.

Tab. II. The DUT is driven by the nominal DC input voltage (V_{IN}), while the interference described in the previous sections is superimposed onto the nominal input voltage by means of a bias tee. Conventional DPI setups comprise of a continuous-wave RF generator cascaded with an RF amplifier. In this work, the interference signal is generated using an Arbitrary Waveform Generator (AWG) [18], which allows the synthesis of non-standard waveforms like that resulting from the substrate coupling. The DUT response is evaluated by monitoring its output voltage (v_{OUT}). Since the nominal input is DC, the output is expected to be constant; however, the applied modulations introduce a time-varying component. Accordingly, v_{OUT} can be expressed as

$$v_{OUT} = V_{OUT} + v_{out}. \tag{5}$$

where V_{OUT} represents the DC component of the output voltage and v_{out} is its time-varying component.
The output voltage in the presence of a switching interference applied at $t_0 = 0$ s, with carrier frequency f_c = 10 MHz, is shown in Fig. 5. In this figure, P_{in} = -7 dBm represents the nominal interference power derived from the substrate-coupling model, whereas the higher level (P_{in} = -3 dBm)

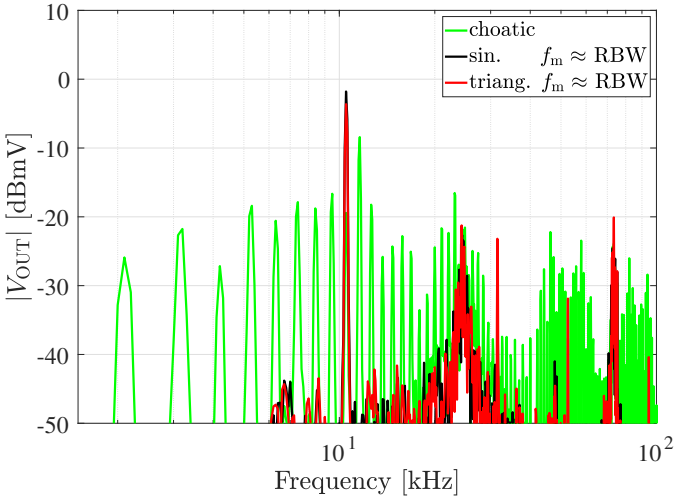

Fig. 6: Frequency spectrum of v_{OUT} with the input interference modulated with different profiles, with P_{in} = - 3 dBm.

TABLE III: Spectral Analysis Results

Modulation	$\overline{v_{out}^2}$ (over R = 1 Ω) [µW]		
	< 9 kHz	9 kHz $\leq$ f $\leq$ 11 kHz	< 100 kHz
sin.	0.01	1.37	1.45
triang.	0.01	0.89	1.01
chaotic	0.17	0.07	0.93

results from the maximum output voltage swing of the AWG used in the experimental setup. The black traces in Fig. 5 show the DUT output voltage when the switching interference is applied without spread-spectrum modulation (unmodulated case). The same figure reports, from top to bottom, the output responses obtained with sinusoidal, triangular, and chaotic modulation, each compared with the unmodulated reference waveform. In the unmodulated case, the output voltage exhibits only a DC shift with respect to the nominal value. When SSM is applied, the output still shows a DC offset, but an additional time-varying component appears. Similar behavior was observed when the same modulations were applied to different carrier frequencies and modulation frequencies.
From the time-domain measurements, the demodulated output voltage appears approximately periodic, with a period that depends on the modulation frequency. To better illustrate this point, the magnitude of the output voltage spectra ($|V_{OUT}|$) for sinusoidal (red), triangular (black), and chaotic (green) modulation are shown in Fig. 6. A spectral component at f_m is visible for both sinusoidal and triangular modulation. Interestingly, the chaotic modulation spreads the frequency components of v_{OUT} over a wider bandwidth, increasing the noise on the analog channel. This behavior can be further quantified by evaluating the mean-square value of v_{out}. For a continuous time signal, the mean-square value (MSV) is defined as

$$\overline{v_{out}^2} = \frac{1}{T}\int_0^T v_{out}^2 dt. \tag{6}$$

According to Parseval's theorem, the MSV can be equivalently evaluated in the frequency domain from the power spectral density (PSD) of the signal. Since the spectral analysis is performed through an FFT, the discrete form is used

$$\overline{v_{\text{out}}^2} = \sum_{k=0}^{N} S_{\text{V}}[k]\Delta f, \tag{7}$$

where S_{V} is the discrete PSD of v_{out} and Δf is the spectral resolution of the FFT. In the following, the MSV is expressed in units of power assuming a reference resistance R = 1 Ω, so that voltage mean-square value and power numerically coincide. The power over different frequency bands is reported in Tab. III. Although sinusoidal and triangular modulation concentrate the spectral power within a narrower bandwidth, the total demodulated energy remains comparable for all three modulation schemes.

To gain further insight into the OpAmp demodulation of spread-spectrum–modulated interference, a measurement campaign was performed. In particular, the impact of the incident power and the carrier frequency was investigated. The $|V_{\text{OUT}}|$ at f_{m} for carrier frequencies between 2 and 10 MHz, using the optimal modulation index, is shown in Fig. 7. Results are shown for P_{in} = –10 dBm. The results indicate that the demodulation increases with incident power, whereas it is only marginally affected by the carrier frequency.

Finally, the role of the frequency deviation (Δf) was investigated. Such parameter is commonly chosen empirically as a trade-off between DC/DC performance degradation, for which small values of Δf are preferred, and achieving effective EMI reduction, which instead requires larger Δf. With the modulation frequency fixed, Δf is changed between 100 kHz and 1 MHz. The corresponding amplitude of the spectral component at f_{m}, evaluated for different carrier frequencies, is reported in Fig. 8. Results show a nearly linear increase in the amplitude of the demodulated component with Δf for all the considered modulation schemes, indicating that excessive Δf values significantly increase the noise affecting the analog channel.

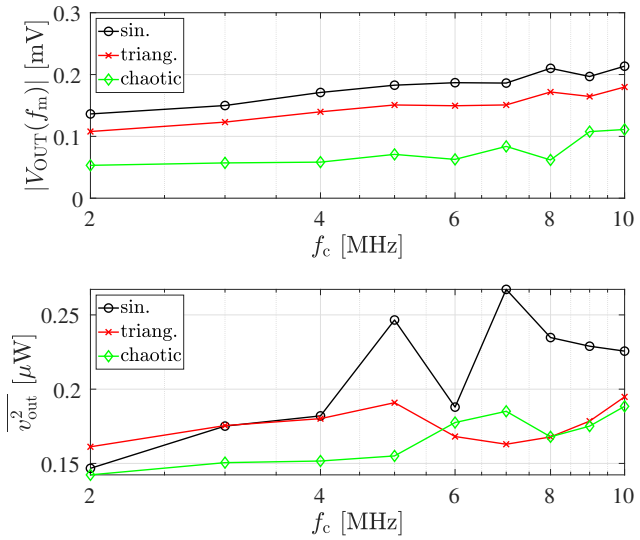

Fig. 7: Amplitude of v_{OUT} at the modulation frequency and demodulated power versus the carrier frequency, with $f_{\text{m}} \approx$ RBW and P_{in} = -10 dBm.

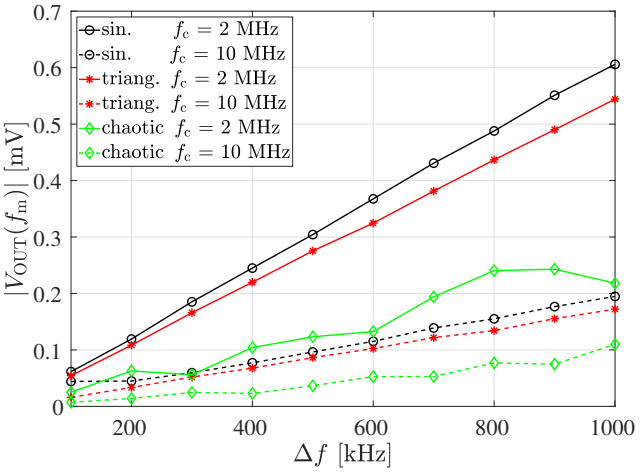

Fig. 8: Amplitude of v_{OUT} at the modulation frequency versus the frequency deviation for different carrier frequency, with $f_{\text{m}} \approx$ RBW and P_{in} = -10 dBm.

VI. Conclusions

In this paper, the susceptibility of OpAmps to spread-spectrum-modulated switching-noise interference applied at the input pin was experimentally investigated. Representative input-referred interference waveforms were first obtained from the time-domain analysis of substrate-coupled switching noise in power ASICs and subsequently shaped using sinusoidal, triangular, and pulse-amplitude (PAM) modulation to emulate realistic disturbances.

The experimental results demonstrate that the investigated amplifier demodulates the interference, generating in-band components that directly corrupt the nominal output signal, leading to a reduction in the signal-to-noise ratio (SNR). Spectral analysis shows that sinusoidal and triangular modulations produce narrowband demodulated components, mainly concentrated around the modulation frequency, whereas PAM modulation results in a broader spreading of the demodulated energy. Consequently, the impact on the output voltage depends on the adopted modulation scheme: narrowband modulations tend to introduce discrete spurious tones, while chaotic PAM modulation increases the in-band noise floor.

Furthermore, the carrier frequency and frequency deviation have been shown to influence the amplitude of the demodulated component, thereby affecting the resulting SNR. From a system-design perspective, these results highlight that, although spread-spectrum modulation is effective in reducing EMI peaks, it may degrade analog circuit performance by introducing additional noise within the signal bandwidth.

REFERENCES

[1] A. Afzali-Kusha, M. Nagata, N. K. Verghese, and D. J. Allstot, "Substrate Noise Coupling in SoC Design: Modeling, Avoidance, and Validation," *Proceedings of the IEEE*, vol. 94, no. 12, pp. 2109–2138, Dec. 2006.

[2] P. Schröter, S. Jahn, and F. Klotz, "Improving the immunity of smart power integrated circuits by controlling RF substrate coupling," in *2011 IEEE International Symposium on Electromagnetic Compatibility*, Aug. 2011, pp. 45–50.

[3] V. Tomasevic, A. Boyer, and S. Ben Dhia, "Bandgap failure study due to parasitic bipolar substrate coupling in Smart Power mixed ICs," in *2015 10th International Workshop on the Electromagnetic Compatibility of Integrated Circuits (EMC Compo)*, Nov. 2015, pp. 34–38.

[4] R. Secareanu, S. Warner, S. Seabridge, C. Burke, J. Becerra, T. Watrobski, C. Morton, W. Staub, T. Tellier, I. Kourtev, and E. Friedman, "Substrate coupling in digital circuits in mixed-signal smart-power systems," *IEEE Transactions on Very Large Scale Integration (VLSI) Systems*, vol. 12, no. 1, pp. 67–78, Jan. 2004.

[5] M. Badaroglu, M. van Heijningen, V. Gravot, J. Compiet, S. Donnay, G. Gielen, and H. De Man, "Methodology and experimental verification for substrate noise reduction in CMOS mixed-signal ICs with synchronous digital circuits," *IEEE Journal of Solid-State Circuits*, vol. 37, no. 11, pp. 1383–1395, Nov. 2002.

[6] J. Fan and T. Harrison, "Substrate switching noise analysis and layout/circuit considerations in monolithic power converters," in *2012 IEEE Energy Conversion Congress and Exposition (ECCE)*, Sep. 2012, pp. 2610–2615.

[7] F. Pareschi, R. Rovatti, and G. Setti, "EMI Reduction via Spread Spectrum in DC/DC Converters: State of the Art, Optimization, and Tradeoffs," *IEEE Access*, vol. 3, pp. 2857–2874, 2015.

[8] F. Fiori, "Susceptibility of Smart Power ICs to Radio Frequency Interference," *IEEE Transactions on Power Electronics*, vol. 29, no. 6, pp. 2787–2797, Jun. 2014.

[9] F. Lin and D. Chen, "Reduction of power supply EMI emission by switching frequency modulation," *IEEE Transactions on Power Electronics*, vol. 9, no. 1, pp. 132–137, Jan. 1994.

[10] A. Bendicks, T. Dörlemann, C. Krause, and S. Frei, "Matlab/octave function to evaluate time-domain signals according to the measurement bandwidth and average/peak detector of emi test receivers," 2022.

[11] P. Wambacq and W. M. Sansen, *Distortion analysis of analog integrated circuits*. Springer Science & Business Media, 2013, vol. 451.

[12] F. Fiori and P. Crovetti, "Investigation on RFI effects in bandgap voltage references," *Microelectronics Journal*, vol. 35, no. 6, pp. 557–561, Jun. 2004.

[13] O. Aiello and F. Fiori, "On the Susceptibility of Embedded Thermal Shutdown Circuit to Radio Frequency Interference," *IEEE Transactions on Electromagnetic Compatibility*, vol. 54, no. 2, pp. 405–412, Apr. 2012.

[14] F. Fiori, "Susceptibility of CMOS Voltage Comparators to Radio Frequency Interference," *IEEE Transactions on Electromagnetic Compatibility*, vol. 54, no. 2, pp. 434–442, Apr. 2012.

[15] F. Fiori, "On the Susceptibility of Chopper Operational Amplifiers to EMI," *IEEE Transactions on Electromagnetic Compatibility*, vol. 58, no. 4, pp. 1000–1006, Aug. 2016.

[16] F. Fiori, "EMI-Induced Distortion of Baseband Signals in Current Feedback Instrumentation Amplifiers," *IEEE Transactions on Electromagnetic Compatibility*, vol. 60, no. 3, pp. 605–612, Jun. 2018.

[17] *Integrated circuits - Measurement of electromagnetic immunity, 150 kHz to 1 GHz - Part 1: General conditions and definitions*, Standard 62 132, Feb. 2006.

[18] Keysight Technologies, *M8190A Arbitrary Waveform Generator – User's Guide*, https://www.keysight.com/us/en/assets/9018-03651/user-manuals/9018-03651.pdf, Apr. 2024, publication number M8190-91030. [Online]. Available: https://www.keysight.com/us/en/assets/9018-03651/user-manuals/9018-03651.pdf